A combined inversion of Rayleigh wave dispersion and 2-D resonance frequencies

D. Roten and D. Fäh

Institute of Geophysics, ETH Hönggerberg, 8093 Zürich, Switzerland. E-mail: daniel.roten@sed.ethz.ch

SUMMARY

Shear wave velocities of the sediment fill of a deep Alpine valley are estimated from ambient noise recorded on linear and circular arrays. We propose a combined inversion of 2-D resonance frequencies identified from site-to-reference spectral ratios and Rayleigh wave dispersion curves obtained from frequency-wavenumber analysis. The method is tested on synthetic noise data and on noise recorded at three sites in the Rhône valley in Southern Switzerland. Previous studies have shown that 2-D resonance dominates the ambient vibration wavefield at low frequencies at the investigated sites. Inversion techniques which assume that the noise wavefield consists mainly of horizontally propagating surface waves will, therefore, fail to resolve shear wave velocities at depths below around 500 m. We show that standard techniques lead to an overestimation of shear wave velocities at depth when applied to synthetic and observed ambient noise. The combined inversion is able to resolve the shear wave velocities in the initial velocity model when applied to synthetic noise records. Application of the method to observed ambient noise improves resolution at depth and yields realistic shear wave velocities for the lower part of the sediment fill.

Key words: Rhône valley, sedimentary basin, seismic array, seismic noise, shear wave velocities, spectral analysis.

GJI Seismology

1 INTRODUCTION

The impact of local ground motion amplification on earthquake damage was demonstrated during many recent damaging earthquakes. In some cases, observed ground motion amplification and increased damage was explained with 1-D analysis of the soil column, for example, for the 1989 Loma Prieta earthquake (e.g. Hough *et al.* 1990). Other observations highlighted the importance of 2-D effects, which may cause higher amplification. A well-known example is the basin-edge effect responsible for the damage belts reported after the 1995 Kobe earthquake (Kawase 1996).

Many cities are located along river valleys on soft unconsolidated sediments, a very common example of a 2-D structure. Numerical simulations have shown for long that 2-D effects may contribute significantly to the seismic response of such sediment-filled valleys. Edge-generated surface waves are the dominant effect in rather shallow valleys, while a 2-D resonance pattern develops in deeper basins (Bard & Bouchon 1980a,b, 1985).

In the framework of the SHAKE-VAL project, we are studying earthquake site effects in the Rhône valley (Fig. 1), a deep sedimentary basin in Southern Switzerland. In a previous numerical study performed for the city of Sion, Frischknecht & Wagner (2004) found that 2-D resonance will cause an amplification significantly higher than the expected 1-D value. However, a quantification of ground motion amplification with such simulations is only possible if a realistic geophysical model of the subsurface structure is available.

Because the amplification is caused by the trapping of S- and surface waves in the sediment, the shear wave velocity is the most important parameter of the geophysical model. Due to growing concern about sediment-induced site effects, methods to estimate shear wave velocities from microtremor array recordings are becoming increasingly popular in seismic hazard assessment. (e.g. Asten *et al.* 2005; Bard *et al.* 2005; Kind *et al.* 2005; Wathelet *et al.* 2005). These methods rely on the assumption that the observed noise wavefield consists mainly of horizontally propagating surface waves, which allows measurement of Rayleigh wave phase velocities using either frequency-wavenumber (e.g. Capon 1969) or spatial autocorrelation (SPAC) techniques (Aki 1957). Under the assumption that the structure underneath the array can be approximated by flat horizontal layers, the Rayleigh wave phase velocity is inverted for the shear wave velocity. This 1-D assumption imposes problems when the method is applied to more complicated 2-D and 3-D sites, like deep sediment-filled valleys. However, methods to estimate shear wave velocities at such sites would be especially desirable, because the even higher amplification caused by such 2-D or 3-D structures was demonstrated in many numerical experiments.

The valley geometry at the investigated sites (Fig. 2) is well know from high-resolution reflection seismic profiles performed during a previous research project (Pfiffner *et al.* 1997) and from gravimetric studies (Rosselli 2001). The steep slope of the sediment–bedrock interface implies that the 1-D approximation may at best be valid for the upper layers of the sediment fill. Furthermore, the noise
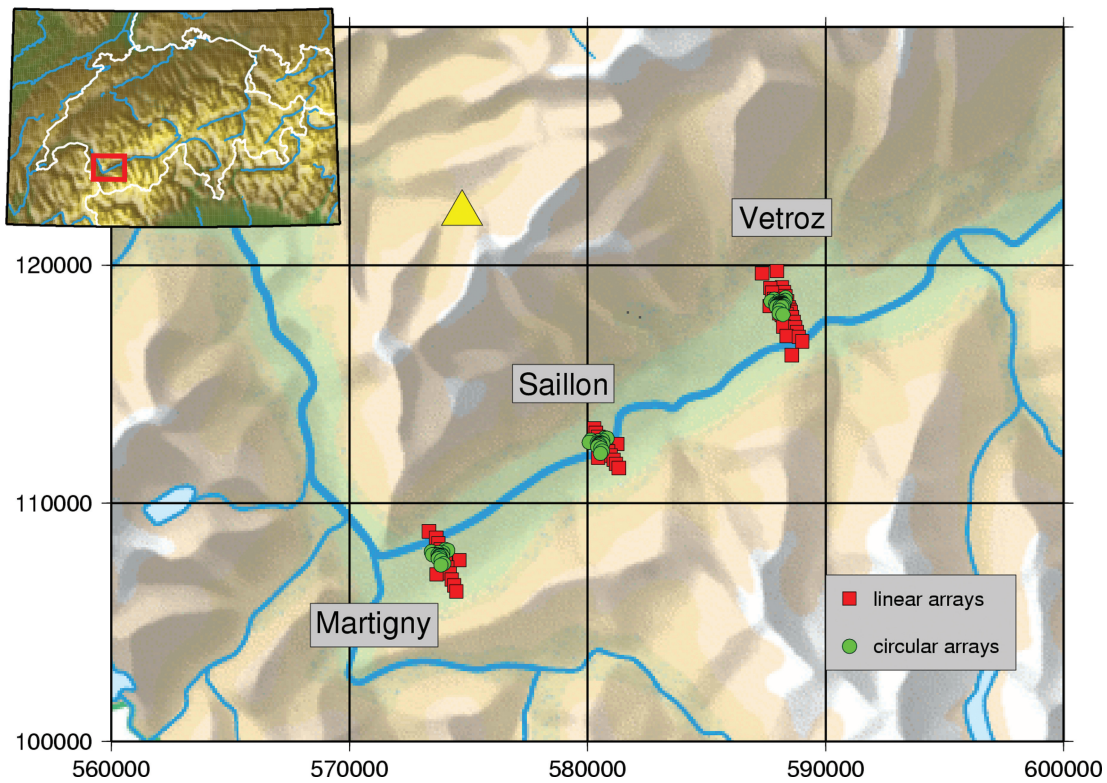
Figure 1. Linear (red) and circular (green) arrays measured in the Rhône valley. The yellow triangle indicates the position of the permanent station GRYON. © 2005 Swisstopo.
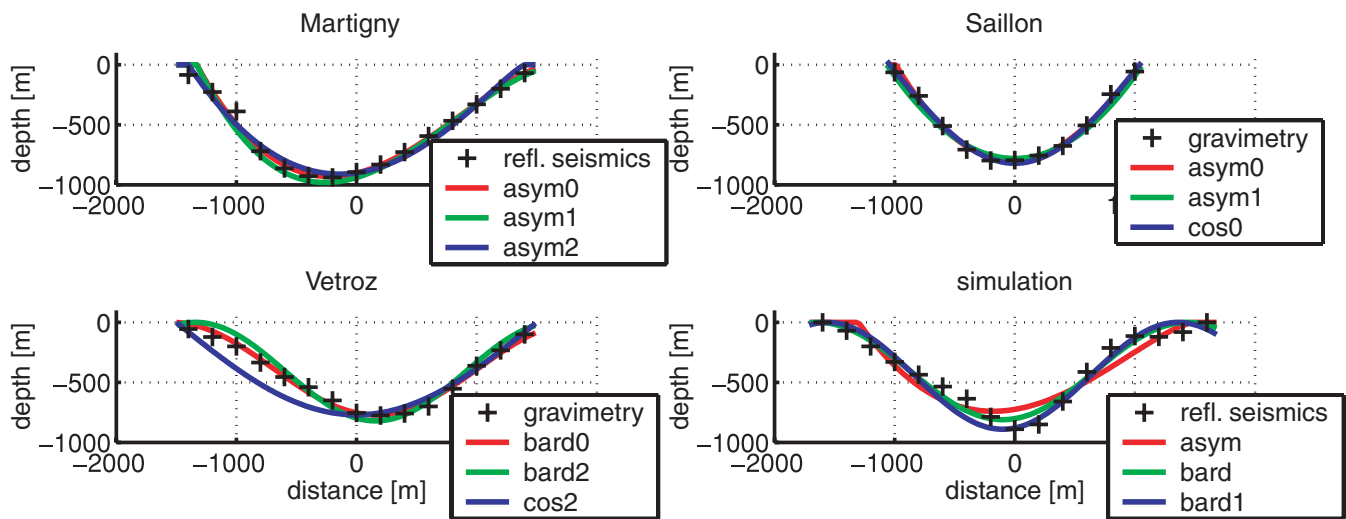
Figure 2. Sediment–bedrock interfaces (*pluses*) reported from reflection seismics (Pfiffner *et al.* 1997) or gravimetry (Rosselli 2001) and different parametrizations (*solid*) used for calculation of 2-D resonance frequencies (Table 2).

wavefield is dominated by standing waves at low frequencies as a consequence of 2-D resonance (Steimen *et al.* 2003; Roten *et al.* 2006). This violates a basic supposition of the microtremor array method, which requires that the noise wavefield be dominated by horizontally propagating surface waves.

In this paper we propose a combined inversion of dispersion curves and 2-D resonance frequencies. The dispersion curves are obtained with circular arrays which sample the upper part of the embanked sediment-filled valleys. To bypass problems caused by the non-1-D structure of the sites and the standing waves at low frequencies, we introduce an approach that combines information about the 2-D resonance behaviour of the sites with observed Rayleigh wave dispersion curves. Our combined inversion aims to find models that explain all observation, and to yield realistic estimations for shear wave velocities that will serve as input parameters for 3-D numerical earthquake simulations. The method is first tested on a synthetic noise data set computed for the Vétroz site and then applied to real noise recorded at three similar sites.

Table 1. Geophysical model of the sediment fill used for the numerical simulation. Depths are in m, v_p and v_s in ms^{-1} and ρ in kgm^{-3} (from Steimen *et al.* 2003).

Depth	v_p	v_s	Q_p	Q_s	ρ	Geological interpretation
0	1700	456	50	25	1900	Deltaic sediments
210	1930	650	50	25	1900	Glaciolacustrine deposits
470	1970	790	50	25	2000	Meltout and reworked till
529	2300	920	50	25	2000	Lodgment and till
584	2050	820	50	25	2000	Subglacial deposit
890	5000	2890	200	100	2500	Hard rock

2 SYNTHETIC NOISE DATA

The ambient noise simulations were performed in the framework of the European SESAME project using a 3-D finite difference method (Moczo & Kristek 2002; Kristek & Moczo 2003). A detailed description of the noise simulation can be found in Roten *et al.* (2006). The geophysical model for the simulation was created by Steimen *et al.* (2003) and corresponds to the sediment–bedrock interface in Fig. 2 (right bottom) with the sediment fill given in Table 1.

Under the assumption that the recorded ambient noise is mostly generated by superficial processes, ambient noise is simulated using a large number of sources on the sediment surface in the valley (Fig. 10 in Roten *et al.* 2006). We will process synthetic noise from a dense circular array with an aperture of 900 m in the valley centre.

3 OBSERVED NOISE DATA

We performed a series of microtremor array measurements at three sites in the Rhône valley (Fig. 1). At each site ambient noise was recorded with two specific array configurations:

(i) For the first configuration, the sensors were aligned in a profile running perpendicular to the valley axis. These linear arrays are used to analyse the resonance behaviour of the valley, as we did for a site near Vétroz in a previous study (Roten *et al.* 2006). The resonance behaviour and the frequencies of the 2-D resonance modes play an important role in the analysis of circular arrays.

(ii) The second type of arrays required a circular receiver layout. This setup is needed to measure the apparent velocity of Rayleigh waves propagating through the array from various directions. In order to sample a range of frequencies, concentric circular arrays with increasing aperture were recorded at most sites.

We deployed three-component sensors with an eigenfrequency of 5 s for all noise measurements. GPS signals were used for time synchronization.

3.1 Observations on linear arrays

For the linear arrays recorded in Martigny, Saillon and Vétroz, we used very similar array geometries. We installed ten receivers on a profile running perpendicular to the valley axis, with a regular spacing of 200–300 m, depending on the valley width (Fig. 1). Two more receivers were placed away from the profile axis near the valley centre. A reference station was deployed on the North side of the valley on bedrock. For the Martigny linear array, the reference site was poorly selected and very noisy. Therefore, the permanent station GRYON from the Swiss Digital Network will be used as a reference (triangle in Fig. 1). The noise wavefield was measured simultaneously on all thirteen receivers during at least an hour.

3.2 Observations on circular arrays

At all three sites, large circular arrays with apertures of about 800 m were recorded. For these arrays, the receivers were arranged around a central station on four concentric circles with radii of about 130, 200, 350 and 400 m, according to a scheme proposed by Kind *et al.* (2005). The array response beampatterns and aliasing limits are given in Fig. 3.

At Martigny, the large array was reshaped to an array of smaller aperture by moving the stations from the two outermost rings to two inner concentric rings with radii of about 30 and 100 m.

At the Vétroz site, the shear wave velocities at higher frequencies were investigated during an additional measurement campaign to sample the structure of the uppermost layers. Three concentric rings of five stations with radii of 16, 40 and 90 m were recorded subsequently, following a recommendation of Bard *et al.* (2005). (Because the array response patterns of the three rings are very similar, only the beampattern of the smallest ring is given in Fig. 3).

4 NOISE DATA PROCESSING

The first step in our noise analysis consists in identification of the 2-D resonance frequencies of the site using linear arrays. Then we extract apparent phase velocities for a range of frequencies from noise recorded on the circular arrays. Results from both linear and circular arrays are then used to invert shear wave velocities of the sediment fill.

4.1 Identification of 2-D resonance

The resonance behaviour of a sediment-filled valley depends on the geometry of the sediment–bedrock interface and the shear wave velocities of the sediment fill. The seismic response of shallow valleys is dominated by the basin-edge effect and by local 1-D resonance. In deep valleys, these edge-generated surface waves interfere with waves propagating vertically, and a 2-D resonance pattern develops. Bard & Bouchon (1985) introduced the *equivalent shape ratio* to distinguish between shallow and deep valleys. It is defined as the maximum valley depth divided by the width over which the sediment-thickness is at least half the maximum depth. The critical shape ratio decreases with increasing velocity contrast between bedrock and sediment fill. If the equivalent shape ratio of a valley is higher than the critical value, the development of 2-D resonance must be expected.

In Fig. 4, the shape ratios of the analysed sites are plotted for ranges of realistic velocity contrasts with the critical shape ratio for the *SH* case. All sites are clearly located in the domain of 2-D resonance.

This 2-D resonance involves three fundamental modes, the *SH*, *SV* and *P* mode. Each of these modes has its own resonance frequency and shows a characteristic pattern of amplification and phase behaviour (Fig. 5). The *SH* fundamental mode involves only the component running parallel to the valley axis. The amplification reaches a maximum in the valley centre. At the *SH* fundamental mode frequency, motion is in phase everywhere in the valley. The *SV* mode involves the vertical component and the direction perpendicular to the valley axis. The amplification shows a central peak on the perpendicular component and a central node on the vertical axis. Motion is in phase in the perpendicular direction, while a phase reversal occurs on the vertical component.

As we reported from a previous study (Roten *et al.* 2006; Steimen *et al.* 2003), these specific patterns of amplification and phase
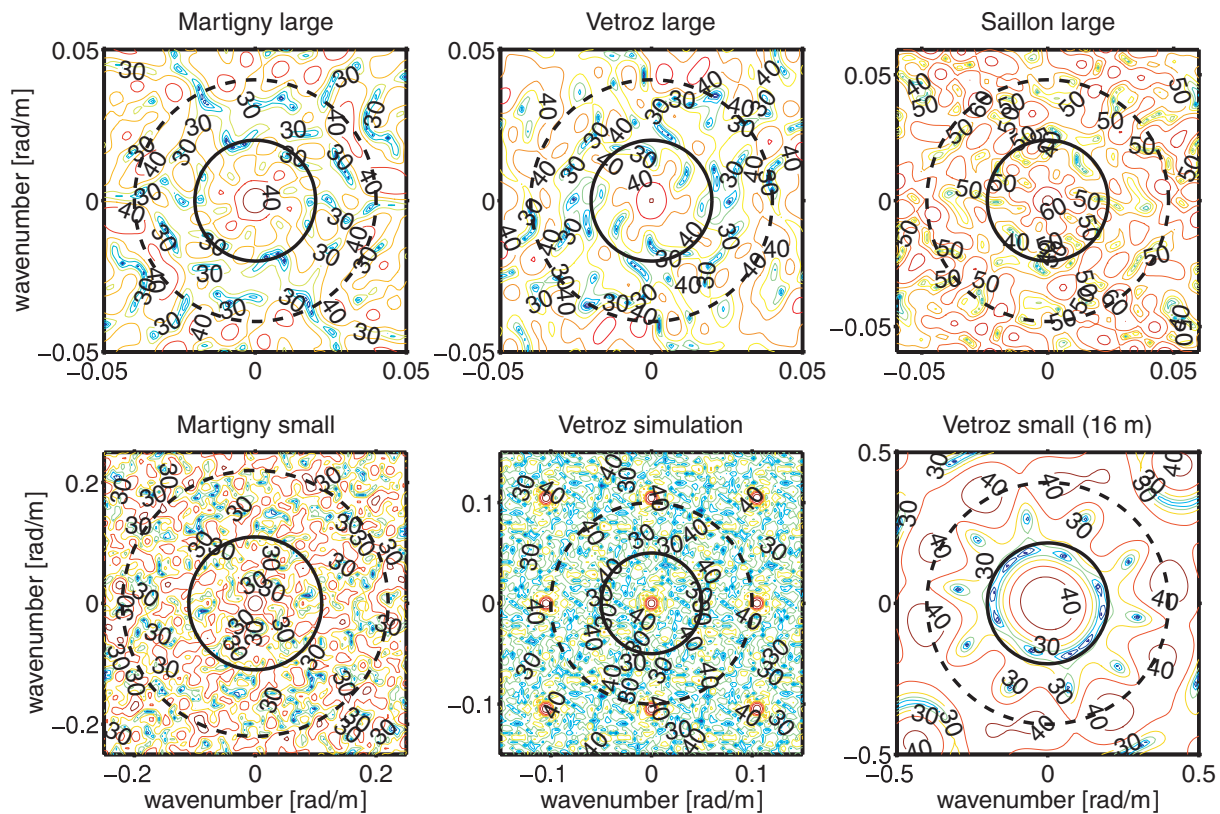
Figure 3. Array response beampatterns for the different small and large aperture circular arrays. Contour lines denote the array response in dB. The wavenumbers of the first aliasing peaks are indicated by the dashed circles, and the wavenumber domains that can be analysed with the individual arrays is within the solid circles.
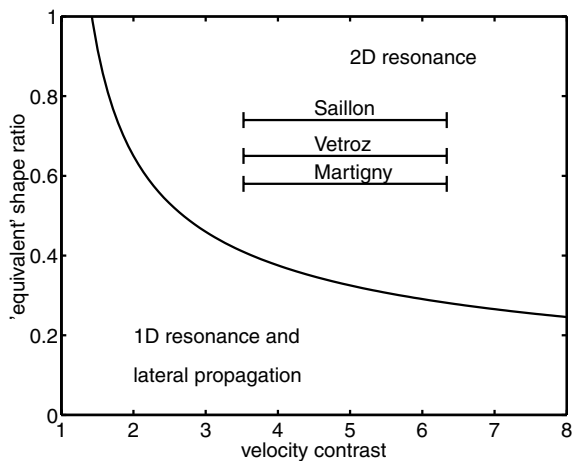
Figure 4. Critical equivalent shape ratio for the *SH* case as a function of velocity contrast and shape ratios of the investigated sites for a range of estimated velocity contrasts (modified from Bard & Bouchon 1985).

behaviour were observed in the ambient vibration wavefield recorded at the Vétroz test site. We will now apply the same method to the linear arrays recorded at Martigny and Saillon.

To identify the 2-D resonance frequencies, we calculate site-to-reference spectral ratios, using the code described in Roten *et al.* (2006). Fourier amplitudes are computed from tapered, 50 per cent overlapping time windows of 80 s length. Then spectral ratios are calculated from the smoothed Fourier amplitudes for each time win-

dow. Average spectral ratios are determined from the individual windows using a weighting scheme.

To eliminate effects of nearby low-frequency disturbances, a simple suppression trigger is applied to each time window after low-pass filtering with a cut-off of 1 Hz. It sets the weight of a time window to zero if the amplitude of any channel at any sensor exceeds a certain threshold value.

4.2 f–k analysis

Noise data recorded on the vertical component on the circular arrays are processed with the high-resolution frequency-wavenumber analysis (Capon 1969) using the algorithm of Kind *et al.* (2005), which is implemented in the continuous array processing software CAP (Ohrnberger *et al.* 2004). The f–k spectra yield angle and apparent slowness of Rayleigh waves propagating through the array from various directions for a set of frequencies. From the f–k spectra, the dispersion curve was extracted for frequencies well above the 2-D resonance frequencies.

4.3 Combined Inversion of Rayleigh wave dispersion curves and 2-D resonance frequencies

Dispersion curves derived from the f–k analysis are inverted for a velocity model with a software developed by Wathelet (2005). The forward problem of calculating the dispersion curves for Love and Rayleigh waves is solved with the method of Dunkin (1965).

The identified resonance frequencies of the different 2-D resonance modes are a function of the valley shape and the shear wave
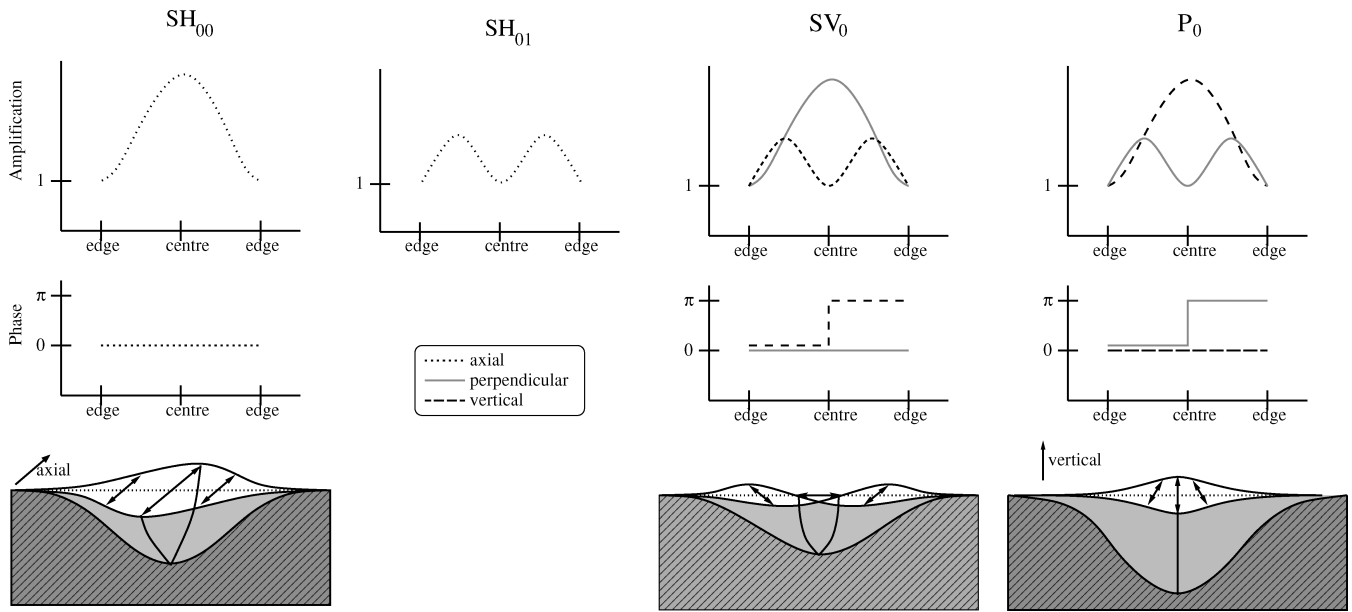
Figure 5. Amplification, phase and particle motion of the three fundamental modes of a sine shaped valley for the corresponding critical shape ratio (modified from Bard & Bouchon 1985; Steimen *et al.* 2003).

velocities in the sediment fill. Since the valley shape of the investigated sites is well known from other studies (Besson *et al.* 1993; Pfiffner *et al.* 1997; Rosselli 2001), we will try to use the observed values of the 2-D resonance frequencies to resolve shear wave velocities in the deeper part of the sediment cover which are not resolved by the array measurements.

We introduce a combined inversion for geophysical models that do not only explain the observed Rayleigh wave dispersion curves, but also the observed 2-D resonance frequencies. The forward problem of calculating the frequencies of the 2-D resonance modes can be solved with a code developed by Paolucci (1999). This program allows to compute the 2-D resonance frequencies of valleys filled with horizontally layered sediments in a fraction of a second. The method is based on Rayleigh's principle, which states that the motion of an undamped elastic system at one of its resonance frequencies can be approximated by a system with a single degree of freedom.

In a 3-D bounded medium, the displacement $s_k(\vec{x})$ of a harmonic vibration with frequency $\omega_0 = 2\pi f_0$ can be described as:

$$s_k(\vec{x}, t) = \psi_k(\vec{x}) e^{i\omega_0 t}, \tag{1}$$

where $\psi_k(\vec{x})$ defines the mode-shape along the direction k (Paolucci 1999). Integrating the kinetic energy over the domain Ω with density ρ and evaluating the maximum gives

$$T_{\max} = -\omega_0^2 \int_\Omega \frac{1}{2} \rho(\vec{x}) \psi_k^2(\vec{x}) \, d\Omega. \tag{2}$$

The strain energy V of the system is given by

$$V(t) = \int_\Omega \frac{1}{2} \sigma_{jl}(\vec{x}) \, \epsilon_{jl}(\vec{x}) \, d\Omega, \tag{3}$$

where ϵ_{jl} is the strain tensor and σ_{jl} the stress tensor.

Energy conservation requires that total elastic energy $V_{\max}$ equal the total kinetic energy in the system $T_{\max}$. Equating expression (2) with eq. (3) yields

$$\omega_0^2 \leq \min_{\hat{\psi}_k} \frac{\int_\Omega \hat{\sigma}_{jl}(\vec{x}) \hat{\epsilon}_{jl}(\vec{x}) \, d\Omega}{\int_\Omega \rho(\vec{x}) \hat{\psi}_k^2(\vec{x}) \, d\Omega}. \tag{4}$$

In the above expression, the exact mode shape $\psi_k(\vec{x})$ has been replaced by a set of admissible approximations $\hat{\psi}_k(\vec{x})$. Because of this approximation, the relation provides only an upper bound for the true resonance frequency ω_0 (Paolucci 1999).

When applied to 2-D alluvial valleys, the interface between valley and bedrock must be parametrized to define the domain Ω and the approximations of the mode shape $\hat{\psi}$. The code by Paolucci (1999) provides four relations, which define sine-shaped, cosine-shaped, elliptic and asymmetric valleys. For cosine-shaped valleys, the sediment–bedrock interface is described by

$$f(x_1, x_3) = \cos\left(\frac{\pi x_1}{2a}\right) - \frac{x_3}{h}, \tag{5}$$

where a is the valley width and h the maximum depth. Sine shaped valleys correspond to the definition used by Bard & Bouchon (1985):

$$f(x_1, x_3) = \cos\left(\frac{\pi x_1}{2a}\right) + \frac{x_3}{h} + \frac{1}{2}. \tag{6}$$

Asymmetric valleys can be approximated with

$$f(x_1, x_3) = \left(1 + \frac{x_1}{a}\right)\left(1 - \frac{x_1}{a}\right)^{\frac{1-\zeta}{1+\zeta}} - (1+\zeta)(1-\zeta)^{\frac{1-\zeta}{1+\zeta}} \cdot \frac{x_3}{h}, \tag{7}$$

where the parameter ζ controls the asymmetry of the interface. To account for uncertainties caused by the parametrization of the sediment–bedrock interface we used different values for each site (Table 2 and Fig. 2).

Application of Paolucci's method to the Vétroz site has shown that the 2-D resonance frequencies calculated from eq. (4) are not more than 0.01 Hz above the values obtained from synthetic ambient noise (Roten *et al.* 2006).

We implemented the method as an additional constraint in the inversion program of Wathelet (2005). For each velocity model created during the inversion process, the velocity profile is combined with the parametrization of the sediment–bedrock interface (Fig. 2 and Table 2), and the corresponding 2-D resonance frequency is computed. Using the L2-norm, the misfit M_{2-D} between the observed and synthetic 2-D resonance frequency is calculated. The

Table 2. Different parametrizations of sediment–bedrock interface for the analysed sites (Fig. 2).

Site	Model name	Valley type	a	h	ζ
Martigny	Asym0	Asymmetric	1480	930	−0.25
	Asym1	Asymmetric	1530	980	−0.30
	Asym2	Asymmetric	1400	910	−0.10
Saillon	Asym0	Asymmetric	1020	800	−0.05
	Asym1	Asymmetric	1065	750	0.00
	Cos0	Cosine	1040	820	
Vétroz	Bard0	Sine	1700	770	
	Bard2	Sine	1500	820	
	Cos2	Cosine	1500	770	
Simulation	Asym	Asymmetric	1120	770	0.20
	Bard0	Sine	1540	810	
	Bard1	Sine	1460	890	

Table 3. Parameter limits for five-layer velocity model used in inversion of synthetic dispersion data. Units are like in Table 1.

Layer	Depth	v_p	v_s	ρ
1	10–300	1700	17–1202	1900
2	300–500	1930	19–1364	1900
3	500–550	1970	19–1393	2000
4	550–600	2200	22–1555	2000
5	770–890	2200	22–1555	2000
6		5000	2890	2500

Table 4. 2-D resonance frequencies [Hz] of the different modes identified at the analysed sites.

site	SV_0	SH_{00}	SH_{01}	SH_{02}
Martigny	0.325	0.29	0.38	0.43
Saillon	0.37	0.32	0.43	
Vétroz	0.35	0.31	0.43	
Simulation	0.34	0.30	0.39	

total misfit M of each model is obtained by combining the misfit between the observed and synthetic dispersion curve M_{DC} and the 2-D misfit M_{2-D}:

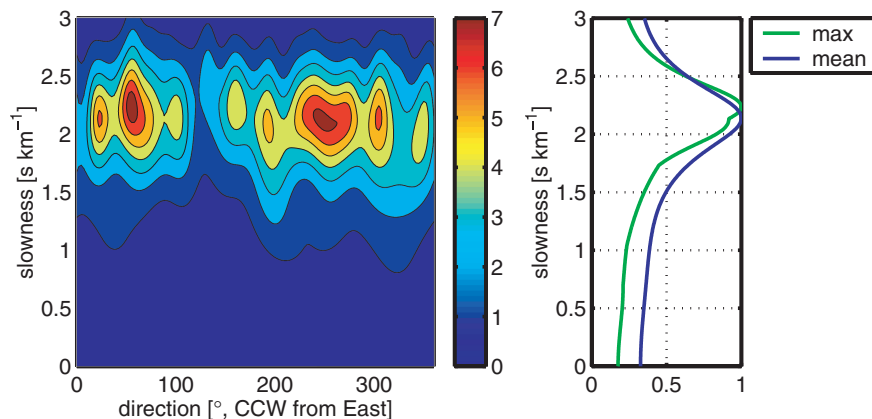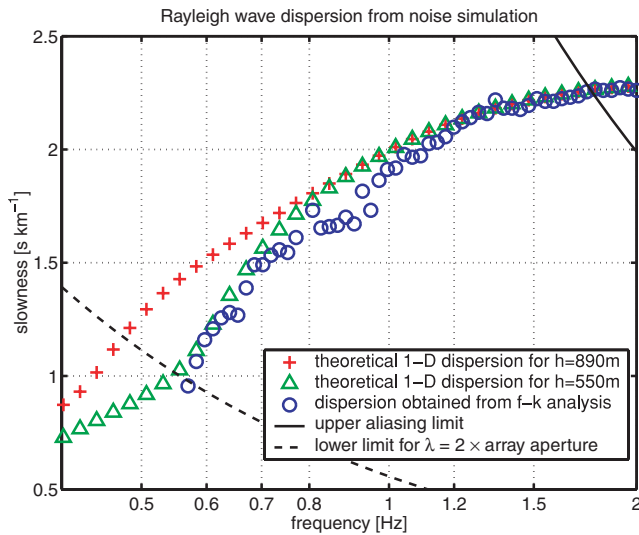$$M = (1 - w) \cdot M_{DC} + w \cdot M_{2-D}. \tag{8}$$

The weighting factor w needs to be adjusted depending on the number of data points to achieve a good fit of both dispersion curves and 2-D resonance frequencies.

4.4 Inversion with the neighbourhood algorithm

For the inversion of shear wave velocities the parameter space is searched with the neighbourhood algorithm introduced by Sambridge (1999a,b). This inversion method has successfully been tested on synthetic and recorded dispersion curves (Wathelet *et al.* 2004).

The neighbourhood algorithm is based on the partition of the solution space into *Voronoi* cells. The global misfit function is approximated by assigning the misfit in the centre of each cell to the whole cell. During each iteration, the sampling of the solution space is refined in regions of low misfit. The algorithm consists of the following stages (Sambridge 1999a):

(i) An initial set of n_s random models is created.
(ii) The misfit of the recent models is calculated. A subset of n_r models with the lowest misfit is selected.
(iii) For each selected model n_r, n_s/n_r new models are generated by a random walk within the cell.

(iv) The algorithm is repeated from step (ii) with the new n_s models for N iterations.

Therefore, the algorithm only needs two tuning parameters: the sample size for each iteration n_s and the number of cells to resample n_r. A high number for n_s and n_r results in explorative sampling of the whole solution space, but requires a larger number of iterations to provide a sufficient number of acceptable models. If low values for n_s and n_r are used the algorithm samples promising regions in a more exploitative way, at the increased risk of getting trapped in local minima.

For the inversion problem described in this text we sought for acceptable velocity models of five to six layers (Table 3). We inverted for the shear wave velocity in each layer and allowed for variations of the layer depth. To reduce the non-uniqueness of the inversion problem we did not allow for shear wave velocities decreasing with depth (Wathelet 2005). Because the *P*-wave velocity does not influence the 2-D resonance frequency when calculated with the method of Paolucci (1999), V_p of each layer was constrained to the values reported from reflection seismic (Pfiffner *et al.* 1997), apart from the shallow uppermost layer for which no value is available from the literature. In order to keep the number of dimensions in the inversion problem low we did not invert for densities but constrained

Figure 6. Left: f–k map obtained from vertical synthetic noise records at 1.26 Hz. The colourbar indicates the array output in dB. Right: normalized maximum and mean over all direction as a function of slowness.

Figure 7. Dispersion curve derived from f–k analysis applied to synthetic ambient noise (circles) compared to theoretical 1-D dispersion curve for the soil column at the maximum depth (pluses) and below the array centre (triangles). The solid line shows the upper resolution limit for the array geometry caused by aliasing. The dashed line shows the lower resolution limit for a maximum wavelength corresponding to twice the array aperture.

them to the estimations derived from gravimetry (summarized in Frischknecht 2000).

With this configuration the number of dimensions ranges between 10 and 13. Following the recommendation of using at least twice the number of dimensions for the sample size we used $n_r = n_s = 50$ to ensure good sampling of the solution space. The number of iterations was set to $N = 1000$, therefore, an ensemble of 50 000 velocity models was created during each inversion.

5 RESULTS FROM SYNTHETIC AMBIENT NOISE

We will start with analysis of the synthetic ambient noise, because results of this simulation may help to understand recorded dispersion curves better.

Site-to-reference spectral ratios calculated from our synthetic noise records are given in Roten *et al.* (2006). The frequencies of SV_0, SH_{00} and SH_{01} were identified at 0.35, 0.30 and 0.39 Hz, respectively (Table 4).

5.1 f–k analysis

Fig. 6 shows an example of f–k spectra obtained from the vertical component of synthetic noise traces. Peaks in the f–k map show incident angle and apparent slowness of Rayleigh waves
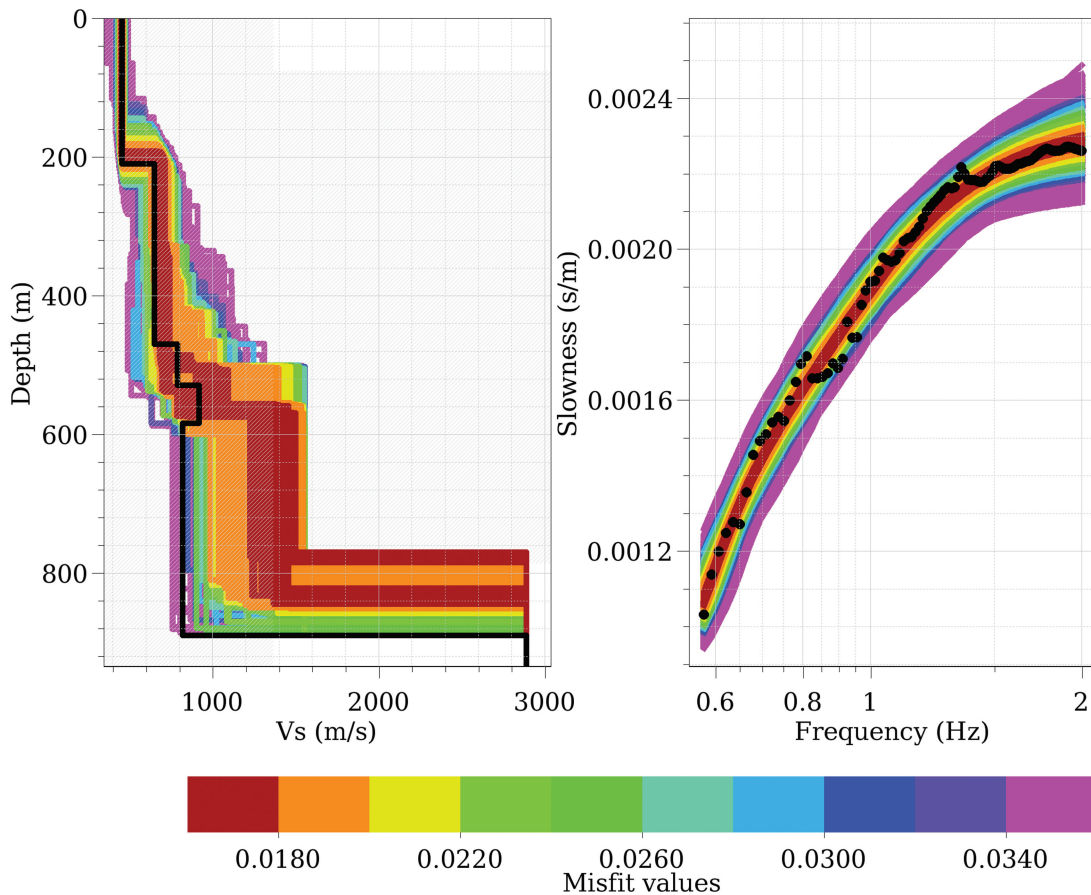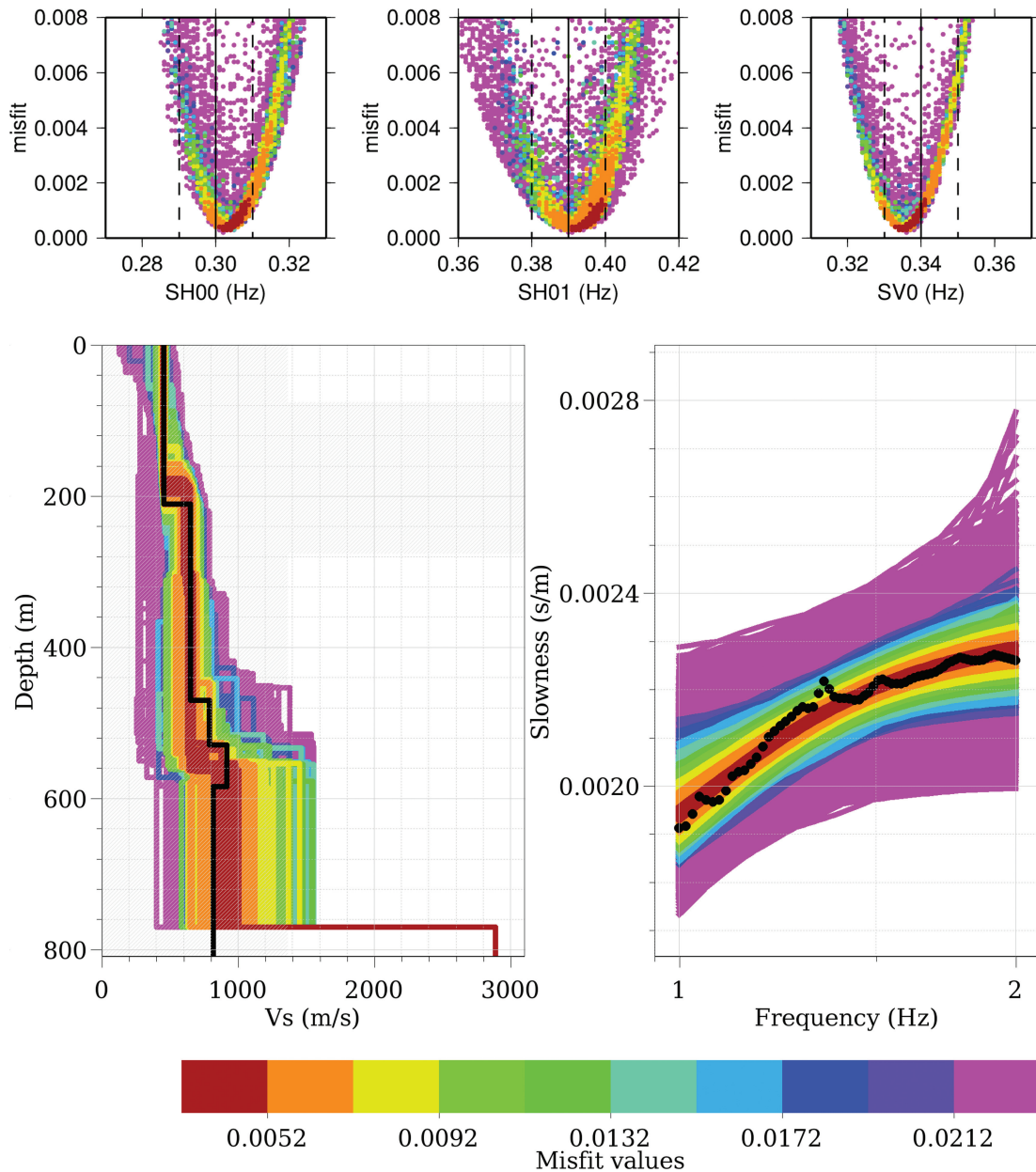

Figure 8. Results of inversion of synthetic dispersion data. Left: obtained *S*-wave velocities. Models with an acceptable misfit level of less than 0.02 are plotted darkred and orange. The true velocity model used for the simulation is indicated by the black solid line. Right: dispersion data (black dots) and modelled dispersion curves (solid colored lines).

propagating through the array from different directions. From these f–k spectra, the dominant apparent slowness for each frequency was selected manually. Fig. 6 (right) shows the maximum and mean over all directions as a function of slowness. For most frequencies, we selected the peak in the mean over all directions as apparent slowness. This approach averages the apparent slowness of waves arriving from different directions, and it results in a slightly smoother dispersion curve than if the absolute maximum in the f–k spectrum is selected. No estimation of uncertainty is available because of the short duration of the synthetic noise time-series.

Fig. 7 compares the dispersion curve derived from f–k analysis (circles) with the theoretical 1-D dispersion curve (pluses) for the soil column at the maximum depth (Table 1). For values above

1.2 Hz, the two curves are very similar. With decreasing frequency, the apparent slowness obtained from the f–k analysis is getting significantly lower than the theoretical value. Triangles in Fig. 7 show the theoretical 1-D dispersion curve for a soil column closer to the valley edge, for a bedrock depth of 550 m. This 1-D dispersion curve shows a reasonable match with the apparent slowness between around 0.6 and 0.7 Hz, but it does not explain the bias in the apparent slowness between 0.8 and 1 Hz. In Fig. 7, the lower resolution boundary of the array is also indicated using a maximum wavelength λ_{max} of twice the largest sensor spacing (e.g. Satoh *et al.* 2001; Ohori *et al.* 2002). The array layout applied on the synthetic noise should, therefore, be large enough to resolve the structure down to at least 0.5 Hz. This implies that the lower apparent slowness obtained from the f–k analysis compared to the 1-D dispersion at the valley

Figure 9. Results of combined inversion of the synthetic dispersion curve and 2-D resonance frequencies with the asymmetrical valley parametrization (Table 2). Top: 2-D resonance frequencies of the different models as a function of 2-D misfit; the color shade gives the total misfit. Bottom: V_s of models and dispersion curves, as for Fig. 8.
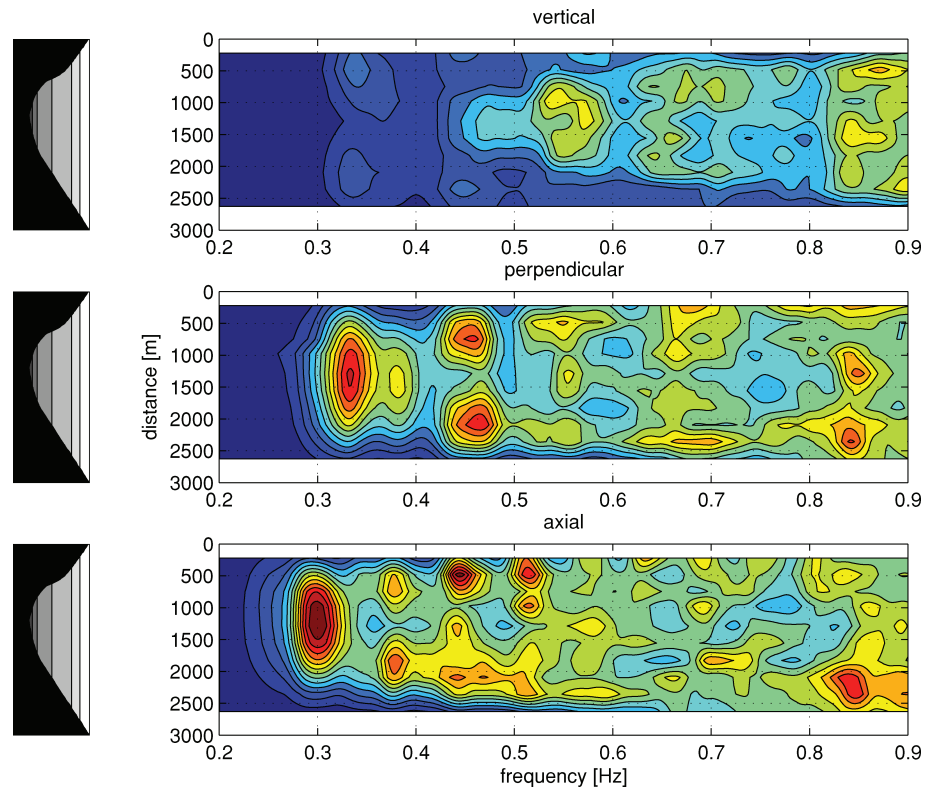
Figure 10. Spectral ratios for Martigny as a function of frequency and distance along the profile axis for vertical (top), perpendicular (centre) and axial (bottom) component.

centre may reflect the influence of lateral bedrock on surface wave propagation.

5.2 Inversion of dispersion curve

Assuming that we have some a priori information of the site, we inverted the dispersion curve obtained from the synthetic noise traces in the frequency range between 0.55 and 2 Hz. The inversion algorithm sought for five-layer velocity models explaining the dispersion curve within the limits given in Table 3.

Fig. 8 shows V_s of the resulting velocity models. The shear wave velocity of the first two layers and the depth of the second layer are well resolved. Shear wave velocities of the sediment fill below around 500 m are systematically overestimated by all models with acceptable misfit. This reflects the fact that the synthetic apparent velocities below 1 Hz are significantly lower than Rayleigh phase velocities expected from 1-D analysis of the sediment fill (Fig. 7).

Nevertheless, the ambient noise array method works still surprisingly well considering the strong non-1-D structure of the input model. The resolution depth of about 500 m corresponds to the classical rule of thumb $h \approx \lambda/3$, where λ is the maximum wavelength of 1500 m obtained from a slowness of about 0.0012 s m^{-1} and a frequency of 0.55 Hz. Using only the dispersion curve above 1 Hz would, therefore, not improve the results but limit the resolution depth to less than 200 m.

5.3 Combined inversion

We will now show results of the combined inversion applied to the synthetic ambient noise dispersion curve. 2-D resonance frequencies for all models were calculated with the three valley parametrizations

from Fig. 2 (right bottom and Table 2). For the combined inversion, the depth of the sediment–bedrock interface is fixed to the value of h in the parametrization in all velocity models.

Because of the discrepancy between theoretical and observed phase velocity below 1.0 Hz (Fig. 7), we only used the dispersion curve between 1.0 and 2.0 Hz for the combined inversion. Fig. 9
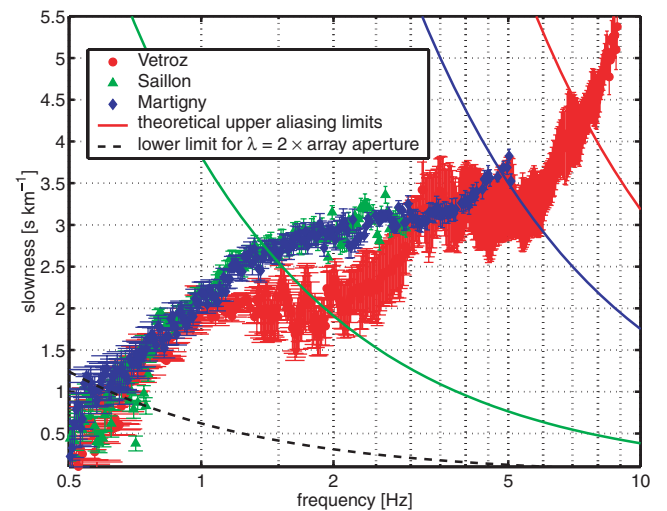
Figure 11. Dispersion curves and standard deviations obtained from large and small aperture arrays. The lower resolution limit corresponds to an array aperture of 800 m. The upper limit was computed from the beampattern of the smallest array at each site.

shows the solution for the asymmetrical valley parametrization. We tried to define an acceptable misfit level such that models with acceptable misfit have computed 2-D resonance frequencies within 0.01 Hz of the observed values (Fig. 9 top).

In comparison with the simple inversion of dispersion curves only, the combined inversion greatly improves resolution at depth and provides a useful estimation of shear wave velocities for the lower sedimentary layers.

For the valley parametrization shown in Fig. 9, the bedrock depth was fixed to 770 m, rather than the 890 m used for the synthetic noise. The other valley parametrizations (Table 2) allow resolution of shear wave velocities to greater depth.

6 RESULTS OF RECORDED AMBIENT VIBRATIONS

Since the combined inversion yields encouraging results when applied to the synthetic ambient noise, we will apply the same method to our recorded noise data.

6.1 2-D resonance behaviour

First, we analyse the resonance behaviour of the sites by calculating site-to-reference spectral ratios from noise recorded with the linear arrays. Fig. 10 shows spectral ratios for the Martigny site as a
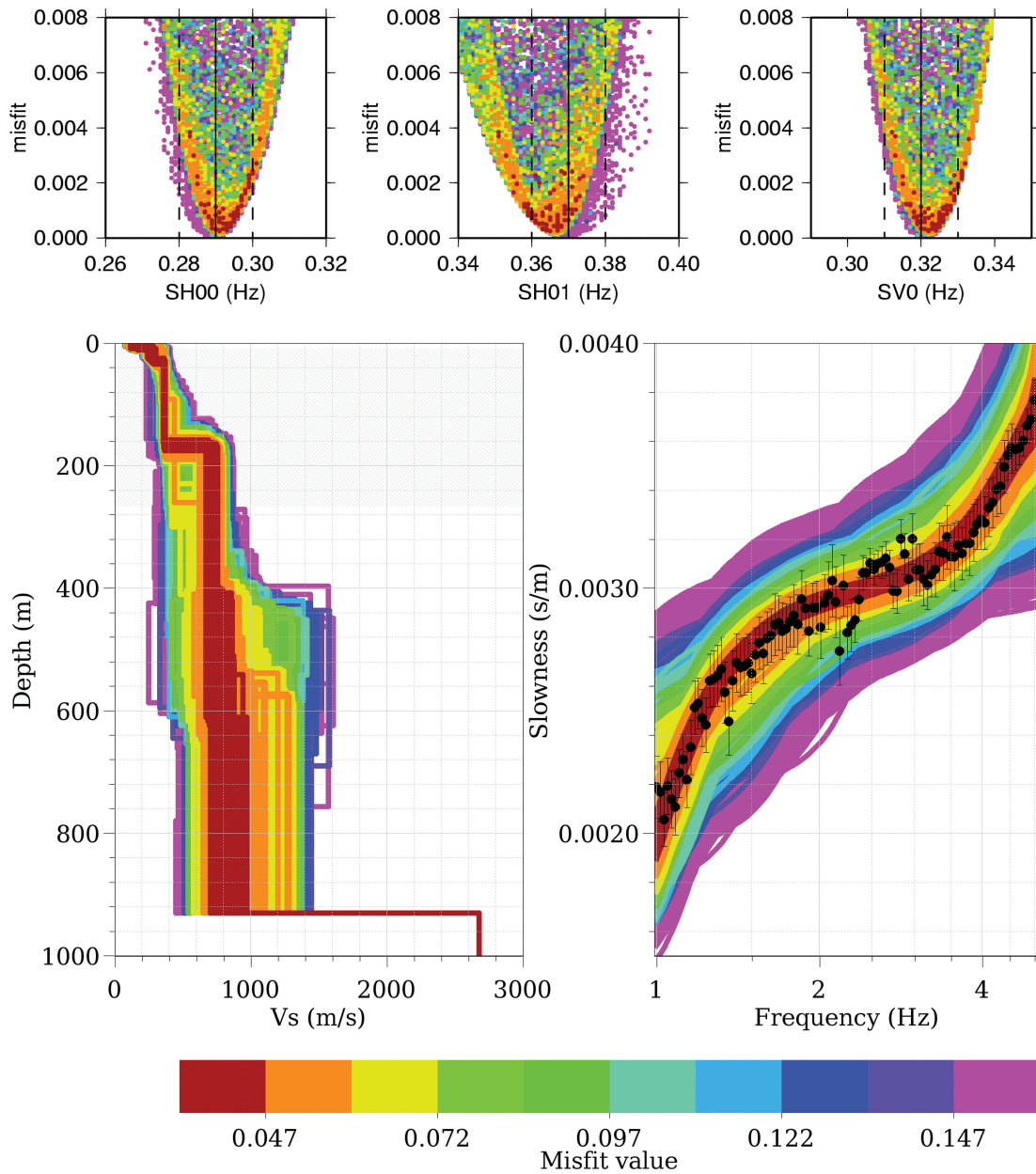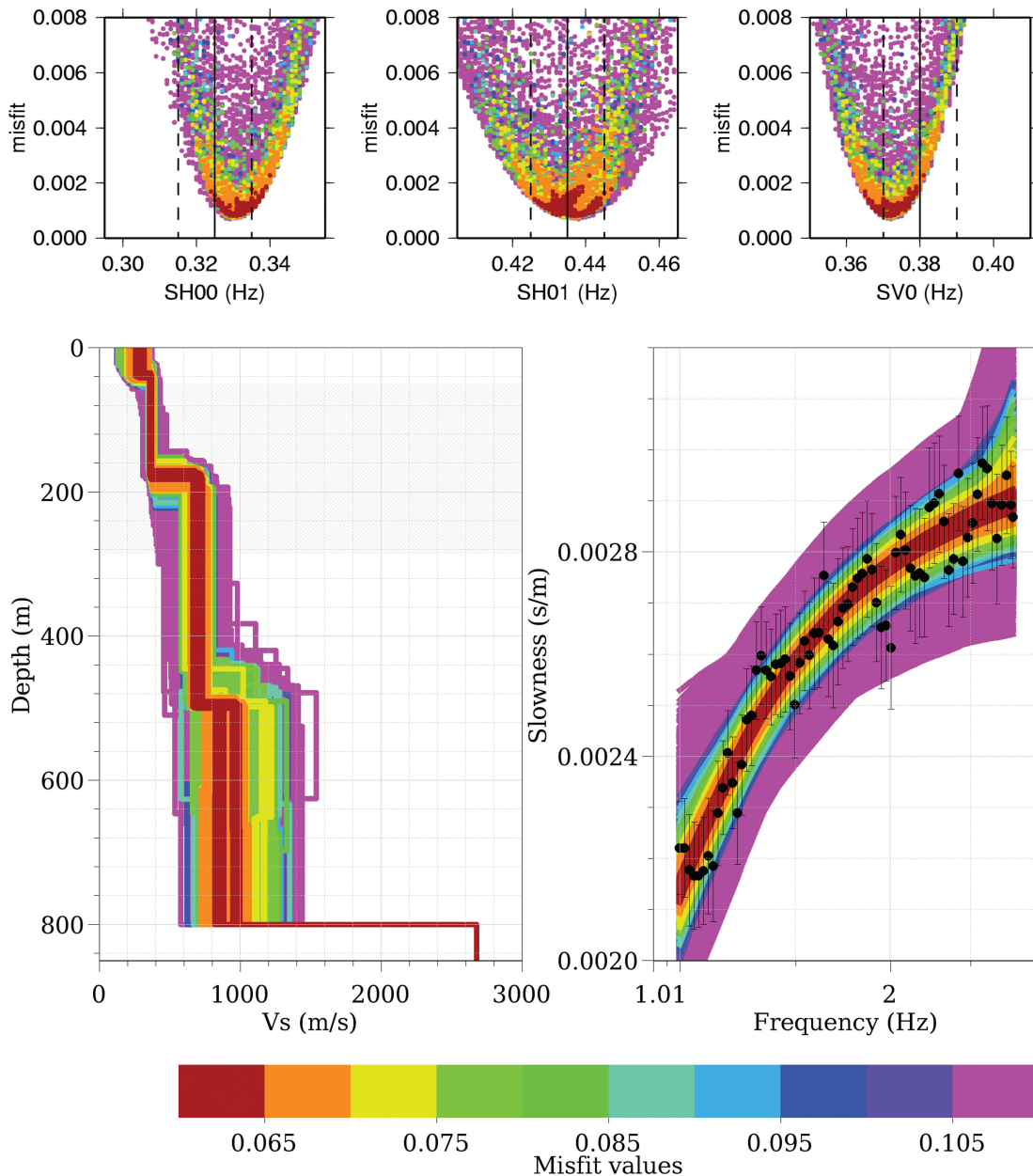

Figure 12. Results of the combined inversion for Martigny obtained with the parametrization 'asym0' (Table 2). Top: 2-D resonance frequencies obtained from the different velocity models as a function of misfit. Bottom: V_s of models and dispersion curves.

function of frequency and distance along the profile axis in a contour plot. The fundamental mode SV_0 can clearly be identified at 0.32 Hz by a central peak on the component perpendicular to the valley axis and by two peaks and a central node on the vertical component. On the axial component, the fundamental and first higher modes of SH resonance are visible at 0.29 and 0.38 Hz. We assigned the three peaks at 0.43 Hz to the second higher mode of SH. Table 4 summaries the resonance frequencies observed at the individual sites. Spectral ratios for the linear profile recorded near Saillon look very similar, but the resonance frequencies are slightly higher here. The resonance frequencies identified at the Vétroz site are also summarized in Table 4. Refer to Roten *et al.* (2006) for spectral ratios of the Vétroz linear arrays.

6.2 f–k analysis

The frequency-wavenumber analysis was applied to the vertical component of all circular arrays recorded at the three sites. For each frequency, the average and standard deviation of the apparent slowness was obtained by computing f–k spectra for a set of overlapping time windows with frequency-dependent window length. The obtained standard deviation is taken into account for misfit calculation between observed and synthetic dispersion curves.

Fig. 11 shows the dispersion curves obtained at the three sites. Dispersion curves for Martigny and Vétroz were combined from results of the different aperture arrays, while the curve for Saillon was obtained only from the large array recorded there. The similarity

Figure 13. Results of the combined inversion for Saillon obtained with the cosine shaped parametrization. Top: 2-D resonance frequencies of the different velocity models as a function of misfit. Bottom: V_s of models and dispersion curves, as for Fig. 12.

in the apparent slowness suggests that shear wave velocities of the Rhône sediments are comparable at the three sites. Especially the curves for Saillon and Martigny are almost identical between 0.7 and 3 Hz; the apparent slowness for Vétroz is clearly lower in this frequency range. At Martigny and Vétroz, the apparent slowness increases quickly for frequencies above 4 and 6 Hz. This may indicate the presense of a shallow low-velocity layer, which was also encountered in nearby boreholes.

It's interesting to note that the temporal stability is much better for Saillon and Martigny (and the dispersion curve below 1.5 Hz for Vétroz), where four concentric rings were recorded simultaneously. The apparent slowness for Vétroz, which was determined from concentric circular arrays recorded subsequently, shows systematically larger standard deviations.

6.3 Inversion of dispersion curves and 2-D resonance frequencies

The parameter limits used for the inversion of observed noise results were similar to the values in Table 3. For Martigny and Vétroz, an additional shallow layer of up to 20 m depth with unknown *P*- and *S*-wave velocity was added. We only inverted for velocities of the top five to six layers, which represent the sedimentary fill of the valley.

6.3.1 Martigny array

Three different valley parametrizations with the asymmetric relation were used (Table 2 and Fig. 2 top right). Results of the parametrization using $a = 1480$, $h = 930$ and $\zeta = -0.25$ are given in Fig. 12.
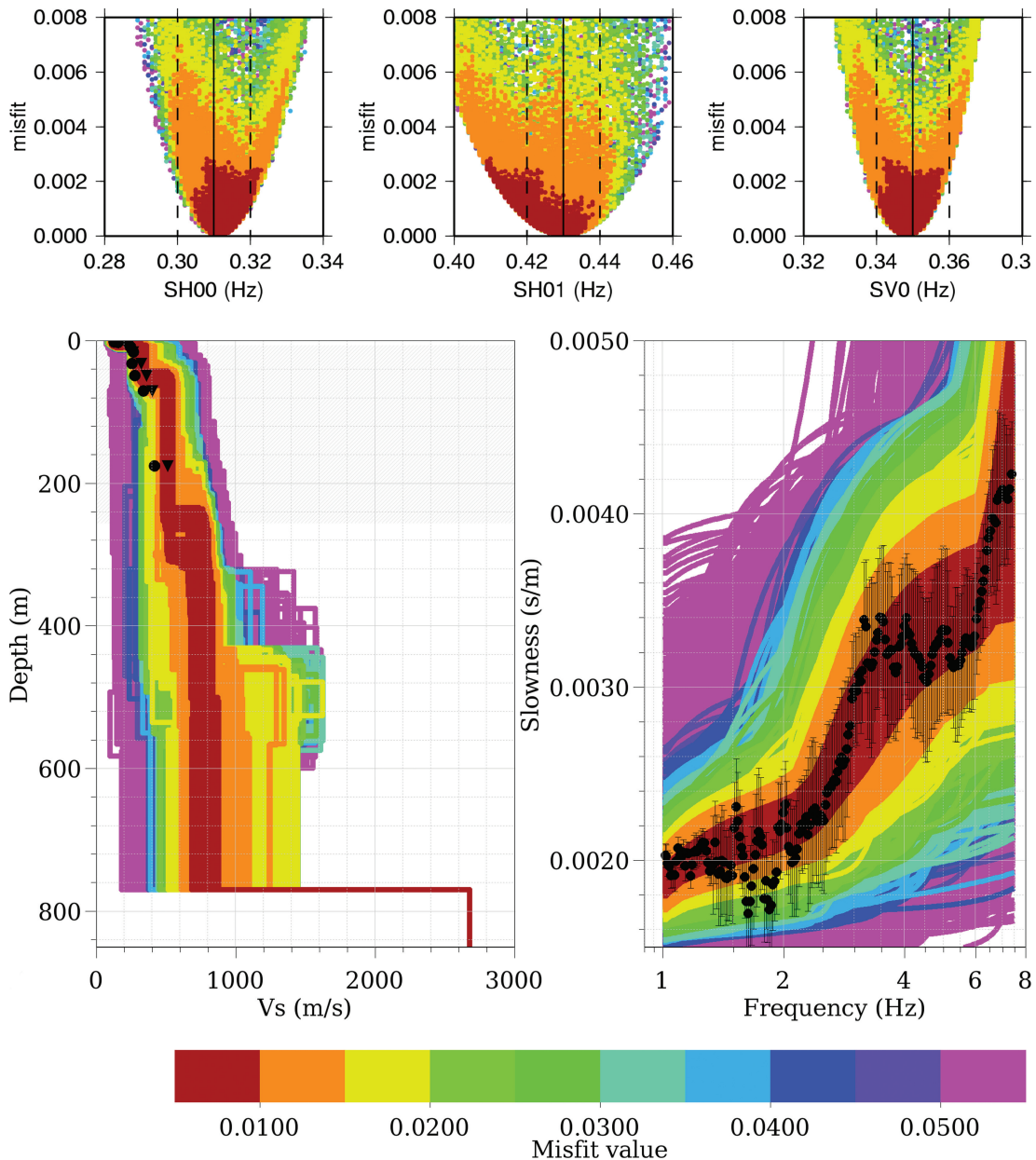
Figure 14. Results of the combined inversion for Vétroz obtained with a cosine-shaped parametrization, $a = 1500$ and $h = 770$. Top: 2-D resonance frequencies of the different models as a function of misfit. Bottom: V_s of models and dispersion curves. The black circles show results of shear wave reflection/refraction measurements, the black triangles shear wave velocities estimated from standard penetration tests (Frischknecht 2000).

The solutions with acceptable misfit are explaining the observed dispersion curve very well. All models exhibit a shallow low-velocity layer of 10 m thickness, with a shear wave velocity of only around $100\,\text{ms}^{-1}$. The next considerable velocity contrast appears at around 180 m depth, where the shear wave velocity rises from around 400 to $700\,\text{ms}^{-1}$. These values are very similar to the geophysical model created by Steimen *et al.* (2003) for Vétroz (Table 1).

All three parametrizations yield shear wave velocities between 600 and $800\,\text{ms}^{-1}$ for the intermediate part of the sedimentary fill. Shear wave velocities of the lowermost layers are sensitive to the chosen valley parametrization and vary between 700 and $1000\,\text{ms}^{-1}$.

The 2-D resonance frequencies of the velocity models with acceptable misfit in Fig. 12 are well within the uncertainty of the observed values for the three analysed modes SH_{00}, SH_{01} and SV_0.

6.3.2 Saillon array

Since no small array was recorded at Saillon, we will not be able to resolve the shallow low-velocity structure at this site. We will only invert for a five-layer model similar to Table 3. Because the linear and circular arrays in Saillon were recorded around 500 m away from the seismic reflection profile, we extracted the sediment–bedrock interface from a 3-D map of the bedrock depth created on the basis of a gravimetric survey (Rosselli 2001).

Fig. 13 shows results of the combined inversion using the cosine-shaped valley parametrization (Table 2). The resulting shear velocities are quite similar to the Martigny site, with a strong velocity contrast appearing at about 180 m depth. Both 2-D resonance frequencies and phase velocities are reproduced well by the velocity models with acceptable misfit.

6.3.3 Vétroz array

Fig. 14 shows results of the combined inversion for Vétroz obtained for a cosine-shaped valley and $a = 1500$, $h = 770$ ('cos2' in Fig. 2

and Table 2). Similar to Martigny, a low-velocity layer of about 10 m thickness can be resolved. A further small velocity contrast appears at around 70 m, where velocities increase from 350 to around $450\,\text{ms}^{-1}$. Shear velocities between 70 and 200 m are, therefore, slightly higher than at Saillon and Martigny, which reflects the lower apparent slowness between 1 and 3 Hz observed in the dispersion curve (Fig. 11). The velocity contrast at about 180 m is less distinct than at Saillon and Martigny, and V_s is slightly lower for depths between 200 and 500 m.

Shear wave velocities in Fig. 14 are compared with results from shallow *S*-wave seismics performed near Vétroz and velocities extrapolated from standard penetration tests (SPT) in the Sion area (Frischknecht 2000). All methods show similar results, though results from seismics and SPT measurements show a more gradual velocity increase for the uppermost layer. These data are only available for depths of less than 200 m; for the deeper part of the sedimentary fill there are no other studies available that we could compare with our results.

6.4 Discussion

Fig. 15 compares results of a simple inversion with results of the combined inversion obtained with all three valley parametrizations for Martigny. The simple inversion was done with the same parameter limits as the combined inversion, but without the additional constraint of fitting the observed 2-D resonance frequencies and with the whole dispersion curve down to 0.60 Hz. With the simple inversion (Fig. 15 a), velocities are well resolved until the interface at around 200 m. Below that interface V_s ranges between 500 and $750\,\text{ms}^{-1}$, and for depths of more than 320 m shear velocities of up to $1600\,\text{ms}^{-1}$ are obtained, which corresponds to the upper limit for this parameter allowed in the inversion.

If we calculate the 2-D resonance frequencies for the best-fitting model obtained by simple inversion for Martigny (grey line in Fig. 15a), we find 0.41 Hz for SV_0 and 0.38 Hz for SH_{00} using
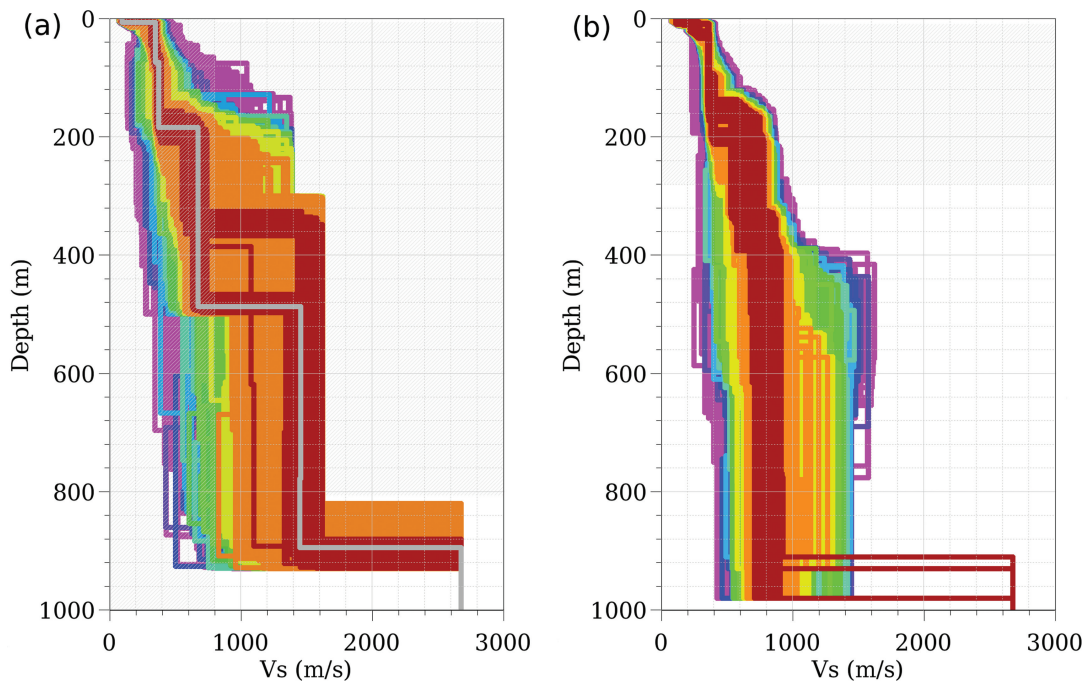
Figure 15. Comparison of simple inversion (a) and combined inversions with all three valley parametrizations (b) for Martigny. Models with an acceptable misfit level are plotted darkred.

combined inversion
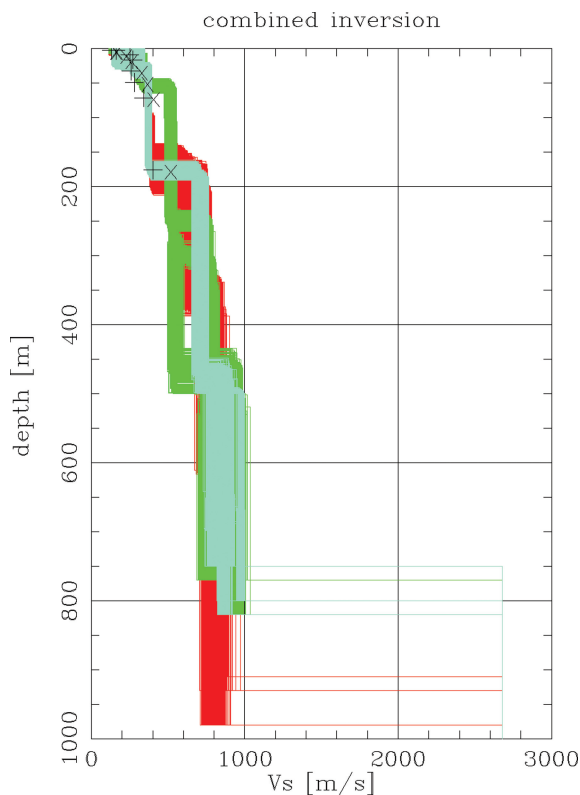
Figure 16. Velocity models with acceptable misfit found for Martigny (red), Saillon (cyan) and Vetroz (green) with all valley parametrizations. The black symbols show shear wave velocities obtained with other methods.

the method of Paolucci (1999). These values are significantly higher than the resonance frequencies observed in spectral ratios calculated from ambient noise (Fig. 10).

Results from reflection seismics show that P-wave velocities in the sediment do not exceed 2400 ms^{-1} (Pfiffner *et al.* 1997). A shear wave velocity of 1600 ms^{-1} would, therefore, require a V_p/V_s ratio of around 1.5, which is unrealistically low for the unconsolidated sedimentary fill of the Rhône valley. Therefore, we have to reject the solutions obtained from simple inversion of dispersion curves, because shear wave velocities in the lower part of the sediment are definitely overestimated.

The acceptable velocity models obtained from the combined inversion (Fig. 15b) scatter significantly less at depths below 320 m, and similar velocities are obtained for all three valley parametrizations in the lower part of the sedimentary fill.

The depth of the interface at 200 m cannot be resolved very accurately and depends on the valley parametrization. This impedance contrast is most likely representing the interface between lacustrine and glaciolacustrine deposits (Table 1), which appears as a strong reflector in seismic reflection profiles (Pfiffner *et al.* 1997).

Fig. 16 compares the acceptable velocity models obtained with all valley parametrizations at the three sites. Shear velocities for Saillon and Martigny are very similar in general, which is in agreement with the similar dispersion curves (Fig. 11). At Vétroz slightly higher velocities are encountered for the top 200 m, and the depth of the next velocity contrast is sensitive to the chosen valley parametrization. Our results suggest that shear wave velocities inside the sedimentary fill are not exceeding 1000 ms^{-1}, but we cannot exclude that they are as low as 700 ms^{-1} down to the sediment–bedrock interface.

Table 5. Shear wave velocities assigned to individual layers from results of the combined inversion (Fig. 16) at all sites. The uncertainties reflect the scatter within the acceptable velocity models and the variability of the velocity at the three sites.

depth (m)	v_s (ms^{-1})	Geological interpretation
0	100–200	Uppermost layer
5–10	320–375	Deltaic sediments
65 –100	385–500	Lacustrine deposits
175–210	500–800	Glaciolacustrine deposits
350–500	700–1000	Meltout and reworked till
550–800	700–1000	Subglacial deposits

In order to create a geophysical model of the Valais area, we tried to assign a shear wave velocity to each layer identified from reflection seismics (Table 5). Our results show that the shear wave velocities in the initial velocity model from Steimen *et al.* (2003, Table 1) represent a good estimate.

7 CONCLUSION

In comparison with the simple inversion of dispersion curves, the additional constraint of the observed 2-D resonance frequencies significantly improves resolution at depth. Inversion of only dispersion curves would lead to poor resolution and overestimation of shear wave velocities at depths below around 300 m due to the 2-D structure of the site. Inversion of the 2-D resonance frequency helps to overcome this problem, and allows to estimate shear wave velocities at depths not accessible by the inversion of only dispersion curves.

REFERENCES

Aki, K., 1957. Space and time spectra of stationary stochastic waves, with special reference to microtremors, *Bull. Earthq. Res. Inst. Tokyo,* **35,** 415–457.

Asten, M., Stephenson, W. & Davenport, N., 2005. Shear-wave velocity profile for holocene sediments measured from microtremor array studies, SCPT, and seismic refraction, *J. Eng. Environ. Geophys.,* **10,** 235–242.

Bard, P.-Y. & Bouchon, M., 1980a. The seismic response of sediment-filled valleys. Part 1. The case of incident SH waves, *Bull. seism. Soc. Am.,* **70**(4), 1263–1286.

Bard, P.-Y. & Bouchon, M., 1980b. The seismic response of sediment-filled valleys. Part 2. The case of incident P and SV waves, *Bull. seism. Soc. Am.,* **70**(5), 1921–1941.

Bard, P.-Y. & Bouchon, M., 1985. The two-dimensional resonance of sediment-filled valleys, *Bull. seism. Soc. Am.,* **75**(2), 519–541.

Bard, P.-Y., Jongmans, D., Ohrnberger, M. & Wathelet, M., 2005. Recommendations for quality array measurements and processing, SESAME deliverable D24.13, SESAME EVG1-CT-2000-00026 project (http://sesame-fp5.obs.ujf-grenoble.fr).

Besson, O., Marchant, R., Pugin, A. & Rouiller, J.-D., 1993. Campagne de sismique-réflexion dans la vallée du Rhône entre Sion et St. Maurice: perspectives d'exploitation géothermique des dépôts torrentiels sous-glaciaires, *Bull. du Centre d'hydrogéologie de l'Université de Neuchâtel,* **12,** 39–58.

Capon, J., 1969. High-resolution frequency-wavenumber spectrum analysis, *Proceedings of the IEEE,* **57**(8), 1408–1419.

Dunkin, J.W., 1965. Computation of model solutions in layered, elastic media at high frequencies, *Bull. seism. Soc. Am.,* **55,** 335–358.

Frischknecht, C., 2000. seismic soil amplification in Alpine Valleys. A case study: the Rhône Valley, Valais, Switzerland, *PhD thesis*, Sections des Sciences de la terre, Université de Genève.

Frischknecht, C. & Wagner, J.-J., 2004. Seismic soil effect in an embanked deep Alpine valley; a numerical investigation of two-dimensional resonance, *Bull. seism. Soc. Am.,* **94,** 171–186.

Hough, S., Friberg, P., Busby, R., Field, E., Jacob, K. & Borcherdt, R., 1990. Sediment-induced amplification and the collapse of the nimitz freeway, *Nature,* **344,** 853–855.

Kawase, H., 1996. The cause of the damage belt in Kobe: 'The basin-edge effect,' Constructive interference of the direct s-wave with the basin-induced diffracted/rayleigh waves, *Seism. Res. Lett.,* **67**(5), 25–34.

Kind, F., Fäh, D. & Giardini, D., 2005. Array measurements of S-wave velocities from ambient vibrations, *Geophys. J. Int.,* **160,** 114–126.

Kristek, J. & Moczo, P., 2003. Seismic-wave propagation in viscoelastic media with material discontinuities: a 3D fourth-order staggered-grid finite-difference modeling, *Bull. seism. Soc. Am.,* **93**(5), 2273–2280.

Moczo, P. & Kristek, J., 2002. FD code to generage noise synthetics, SESAME deliverable D09.02, SESAME EVG1-CT-2000-00026 project (http://sesame-fp5.obs.ujf-grenoble.fr).

Ohori, M., Mobata, A. & Wakamatsu, K., 2002. A comparison of ESAC and FK methods of estimating phase velocity using arbitrarily shaped microtremor arrays, *Bull. seism. Soc. Am.,* **92**(6), 2323–2332.

Ohrnberger, M. *et al.*, 2004. User manual for software package CAP - a continuous array processing toolkit for ambient vibration array analysis, SESAME deliverable D18.06, SESAME EVG1-CT-2000-00026 project (http://sesame-fp5.obs.ujf-grenoble.fr).

Paolucci, R., 1999. Shear resonance frequencies of alluvial valleys by Rayleigh's method, *Earthquake Spectra,* **15**(3).

Pfiffner, O.A., Heitzmann, S., Mueller, S. & Steck, A., 1997. *Deep Structure of the Swiss Alps—Results of NRP 20*, Birkhäuser, Basel.

Rosselli, A., 2001. Modélisation gravimétrique bi- et tridimensionelle du substratum rocheux des vallées alpines, *PhD thesis*, Université de Lausanne.

Roten, D., Cornou, C., Fäh, D. & Giardini, D., 2006. 2D resonances in Alpine valleys identified from ambient vibration wavefields, *Geophys. J. Int.,* **165,** 889–905.

Sambridge, M., 1999a. Geophysical inversion with a neighbourhood algorithm—I. Searching a parameter space, *Geophys. J. Int.,* **138**(2), 479–494.

Sambridge, M., 1999b. Geophysical inversion with a neighbourhood algorithm—II. Appraising the ensemble, *Geophys. J. Int.,* **138**(3), 727–746.

Satoh, T., Kawase, H. & Matsushima, S., 2001. Estimation of S-wave velocity structures in and around the Sendai basin, Japan, using array records of microtremors, *Bull. seism. Soc. Am.,* **91**(2), 206–218.

Steimen, S., Fäh, D., Kind, F., Schmid, C. & Giardini, D., 2003. Identifying 2D resonance in microtremor wave fields, *Bull. seism. Soc. Am.,* **93**(2), 583–599.

Wathelet, M., 2005. Array recordings of ambient vibrations: surface-wave inversion, *PhD thesis*, University of Liège, Belgium.

Wathelet, M., Jongmans, D. & Ohrnberger, M., 2004. Surface wave inversion using a direct search algorithm and its application to ambient vibration measurements, *Near Surf. Geophys.,* **2,** 211–221.

Wathelet, M., Jongmans, D. & Ohrnberger, M., 2005. Direct inversion of spatial autocorrelation curves with the neighborhood algorithm, *Bull. seism. Soc. Am.,* **5**(5), 1787–1800.